UC Irvine
UC Irvine Previously Published Works

Title

15 In vivo multiphoton microscopy of human skin

Permalink

https://escholarship.org/uc/item/79h9t948

ISBN

9783110438987

Authors

Balu, Mihaela
Kelly, Kristen M
Harris, Ronald M
et al.

Publication Date

2018-01-22

DOI

10.1515/9783110429985-017

Copyright Information

Peer reviewed

Mihaela Balu, Kristen M. Kelly, Ronald M. Harris, Karsten König,
Christopher B. Zachary, and Bruce J. Tromberg

15 In vivo multiphoton microscopy of human skin

Abstract: The development of clinical multiphoton technologies has led to new, label-free approaches for non-invasive, in vivo imaging of human skin. Recent studies have shown that multiphoton imaging can be used to assess a wide range of biological processes, including cancer, cellular metabolism, and the effects of skin treatments. The imaging devices *MPTflex* and its earlier version, *DermaInspect*, have been employed in a broad range of clinical applications spanning from characterizing and understanding keratinocyte metabolism to malignant melanoma detection and diagnosis, pigment biology, cosmetic treatments, and skin aging. The promising results indicate that in the near future, real-time non-invasive nonlinear "optical biopsies" can be performed at the bedside.

15.1 Introduction

Microscopic evaluation of skin is required in many areas of dermatology such as diagnosing skin diseases, assessing the effects of cosmetic treatments, and understanding skin function. However, optical imaging of skin is challenging due to the fact that it is relatively thick, scatters light strongly, and has very little contrast. As a result, the standard approach for skin imaging with conventional optical microscopy is to slice it upon fixation, mount and stain the slices on microscope slides, and analyze each slide one at a time. This technique has two main limitations:

(1) It is time consuming and it involves many steps in the process that can be prone to errors.
(2) The tissue needs to be removed from its natural environment; while the overall tissue morphology is preserved during the slicing and staining process, the main features related to tissue functionality such as metabolism, are lost.

Over the past 20 years, optical technologies based on in vivo laser scanning microscopy have been developed to address these limitations. This method utilizes focused illumination of a laser beam to provide access to the submicron scale and raster-scanning across the sample to create high-resolution images. Each image plane (about 2 μm thick) forms an optical section and can be used in reconstructing a 3D-view of the skin by scanning at multiple depths. How laser scanning microscopy (LSM) can overcome high scattering and low contrast of unstained tissue is an area of current research. The scattering limitation has been solved only partially. Using a laser beam as a light source allows for wavelength selection that affects the scattering process. Longer wavelengths are scattered less than shorter wavelengths by a turbid

medium such as skin making near-infrared light (NIR) particularly attractive for LSM techniques. Nevertheless, limited depth penetration in skin due to light scattering remains a major limitation of these techniques and a permanent challenge that is being addressed as the technology advances.

Image contrast of unstained skin tissue, on the other hand, has been improved substantially and is based on different mechanisms corresponding to particular LSM techniques. Among these, reflectance confocal microscopy (RCM) and multiphoton microscopy (MPM) have been the most widely used in research studies related to applications in dermatology. RCM contrast is based on variations in tissue refractive index, which provide gray scale images with submicron resolution. MPM contrast in skin is derived from second-harmonic generation (SHG) of collagen and two-photon excited fluorescence (TPEF) of tissue components such as the cofactors NADH and FAD, elastin, keratin, and melanin.

Due to its dual contrast mechanism, MPM provides multicolor images that distinguish cellular features from the extracellular matrix. MPM imaging is unique among other optical imaging technologies in that it provides 3D, near real-time submicron resolved label-free images of living tissues in their native environment with contrast that closely resembles the histological sections dermatopathologists use for diagnosis. MPM technology has been translated into clinical settings through the development of the MPM-based clinical tomographs, DermaInspect [1] and MPTflex by JenLab GmbH (Jena, Germany). This chapter summarizes the results of the most recent clinical studies in the dermatology field, performed by employing either the DermaInspect or the MPTflex tomographs.

15.2 MPM technology and translation into the clinic

The first experiments using TPEF and SHG laser scanning microscopy were performed in 1990 [2] and 1993 [3], respectively. The first experiments on in vivo TPEF imaging of human skin were performed in the late 1990s [4–6]. TPEF and SHG imaging techniques were combined in a single MPM-based tomograph (DermaInspect, Fig. 15.1 (a)) for in vivo skin imaging in 2003 [1]. This system was developed by JenLab, GmbH (Jena, Germany) and it is CE-marked for clinical use along with its most advanced version MPTflex (Fig. 15.1 (b)), a compact, portable device that features an articulated arm to allow imaging almost any region of the body.

The system consists of a compact Ti:sapphire femtosecond laser, an articulated arm with near-infrared optics, and beam scanning module. The system has two photomultiplier tube detectors for parallel acquisition of two-photon excited fluorescence (TPEF) and second-harmonic generation (SHG) signals. A customized metallic ring taped on the subject's skin attaches magnetically to the objective holder in the articulated arm, minimizing motion artifacts. The images acquired by MPTflex and DermaInspect have a lateral spatial resolution of $\approx 0.5\,\mu m$ and an axial resolution $< 2\,\mu m$. The

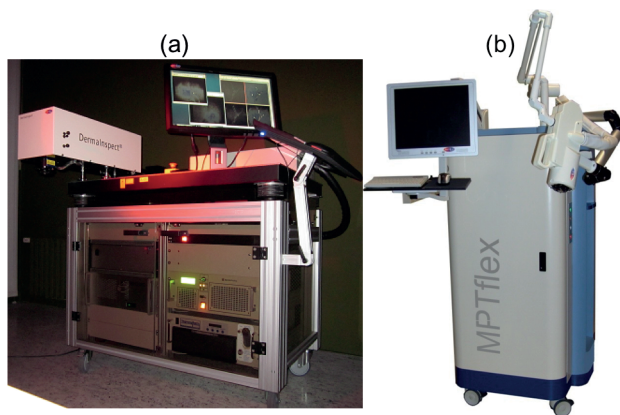**Fig. 15.1:** MPM-based clinical tomographs, (a) DermaInspect and (b) MPTflex.

imaging depth in skin is about 200 μm, depending on the skin or lesion types imaged. The area imaged (field of view) is 250×250 μm^2. The field of view can be increased to a few mm^2 by implementing a mosaic "tiling" feature (acquisition of adjacent fields of view).

MPTflex and its earlier version, DermaInspect, have been employed in a broad range of clinical applications spanning from characterizing and understanding keratinocyte metabolism [7] to skin cancer detection and diagnosis [8–10], pigment biology [11], cosmetic treatments [12], and skin aging [13–16].

15.3 Applications of MPM-based clinical tomographs in dermatology

15.3.1 In vivo MPM imaging of normal skin

Commonly, MPM imaging is used in en-face (horizontal section) mode, but cross-sectional (vertical) sections can also be acquired in real time. Fig. 15.2 shows a representative example of MPM images from normal skin acquired with MPTflex. The en-face images were acquired as a z-stack of horizontal images every 5 μm. En-face images corresponding to different skin layers were selected and shown in Fig. 15.2. The stratum corneum is visualized through TPEF fluorescence from keratin, a thin bright layer on the top surface of the skin in the cross-sectional image and an acellular bright fluorescent layer in the corresponding en-face image. The epidermis shows normally distributed keratinocytes imaged by the TPEF fluorescence from NADH/FAD, keratin and melanin (in the case of pigmented skin). The dermal-epidermal junction (DEJ) is clearly delineated in the cross-sectional view as it separates the basal cell layer from the dermis. Pigmented keratinocytes in the basal
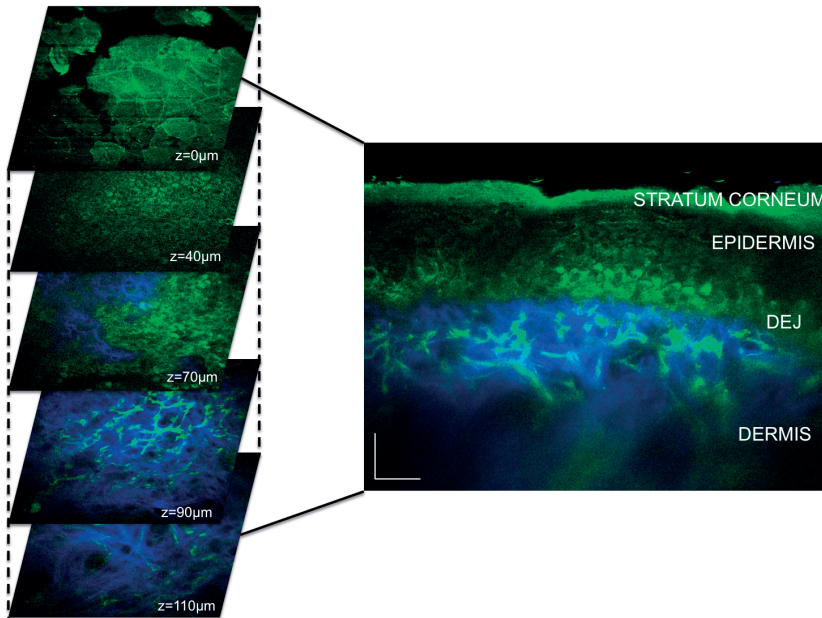
Fig. 15.2: In vivo MPM imaging of normal skin (volar forearm). (Left) MPM horizontal sections (XY scans) at different depths showing images of the stratum corneum ($z = 0\,\mu m$), keratinocytes normally distributed in the stratum spinosum ($z = 40\,\mu m$), the basal cells (green) surrounding dermal papilla (blue) ($z = 70\,\mu m$), collagen (blue) and elastin (green) in the dermis ($z = 90\,\mu m$ and $110\,\mu m$). (Right) Cross-sectional view (XZ scan) corresponding to a vertical plane through the horizontal sections on the left. The image shows the well-delineated layers of the stratum corneum, epidermis, dermalepidermal junction (DEJ) and the superficial dermis.

layer appear as bright fluorescent cells along the DEJ due to their melanin content. In the en-face images of the DEJ, the basal cells are imaged as surrounding the tips of the dermal papillae. Dermal papillae and the dermis are visualized through the SHG signal from collagen and TPEF signal from elastin fibers. Occasionally, blood vessels and capillaries are imaged in the dermis as shown in Fig. 15.2.

15.3.2 In vivo MPM imaging can determine the depth dependent sensitivity of human epidermis to vascular oxygen supply

The reduced nicotinamide adenine dinucleotide (NADH) concentration within mitochondria is closely related to the cellular oxygen supply [7, 18, 19]. Monitoring and imaging the mitochondrial NADH fluorescence, as a way of evaluating the supply of oxygen within cells, has been an area of interest in research over the past 50 years. While most of the pioneering work in this field was based on UV excitation sources, two-photon induced fluorescence employing NIR excitation light has the advantage

of reduced cellular photodamage and improved cell viability, allowing in vivo probing of mitochondrial NADH fluorescence over an extended period of time. MPM allows in vivo imaging of human keratinocytes through the TPEF signal from NADH. In a recent study, we used this device to monitor in vivo and non-invasively the changes in NADH fluorescence of human epidermal cells induced by ischemia through blood-supplied oxygen deprivation [7]. Ischemia-induced changes in NADH fluorescence of keratinocytes in layers close to the stratum basale were compared to NADH fluorescence of keratinocytes from epidermal layers closer to the skin surface. The intensity results recorded as a time series before, during, and after arterial occlusion for epidermal cells in layers close to the stratum basale and skin surface, are shown in Fig. 15.3, along with representative TPEF images at different time points. The results show that ischemia induced by blood-supplied oxygen deprivation is associated with a strong increase in NADH fluorescence of keratinocytes in layers close to the stratum basale, whereas keratinocytes from epidermal layers closer to the skin surface are not affected. This implies that the metabolic processes of keratinocytes in deeper layers such as stratum spinosum and stratum basale are regulated by capillary oxygen supply, whereas the keratinocytes in upper layers such as stratum granulosum are either supplied by atmospheric oxygen [20] or are functionally anaerobic as suggested in previous studies [21].

NADH fluorescence changes were monitored concurrently with changes in tissue oxy- and deoxyhemoglobin concentration during oxygen deprivation using the functional imaging method, spatial frequency domain imaging (SFDI [22]) (Fig. 15.3 (c)). After blood flow was occluded at $t = 3$ min, the tissue deoxyhemoglobin concentration (ctHHb) increased at the expense of oxyhemoglobin (ctO_2Hb), because oxygen was extracted from blood by the epidermal cells and surrounding tissue. The occlusion-induced ischemia reduces the rate of oxidative phosphorylation, resulting in a higher concentration of NADH and higher fluorescence from the epidermal cells that are sensitive to capillary oxygen supply. After the occlusion release at $t = 6$ min, the tissue was rapidly reperfused resulting in an increase in ctO_2Hb and decrease in ctHHb. There was an initial overshoot of the oxy- and deoxyhemoglobin values followed by a return to baseline. These results were similar to previous in vivo measurements of human tissue hemodynamics during arterial occlusion using SFDI [23] and other techniques [24].

The combined MPM/SFDI measurements allowed us to estimate an oxygen consumption rate by basal layer keratinocytes. The rate of decrease in oxyhemoglobin concentration (ctO_2Hb) is related to the rate of oxygen consumption (OC) concentration by:

$$OC = -4\frac{\partial}{\partial t}ctO_2Hb, \qquad (15.1)$$

where the 4 accounts for the hemoglobin to oxygen molar ratio [25]. From the average decrease in oxyhemoglobin concentration of 0.025 µmol/l/s during the arterial occlusion measured by SFDI (Fig. 15.3 (c)), the oxygen consumption rate can be estimated

as 0.1 μmol/l/s by using equation (15.1). By calculating the TPEF imaged volume of the keratinocytes close to the basal layer, the oxygen consumption rate of these cells can be estimated. Therefore, in the TPEF imaged volume of about 200 picoliters containing around 200 cells, the oxygen consumption rate can be estimated to be about 0.035 μmol/10^6 cells/hour. This is the first attempt to measure the oxygen consumption rate by human keratinocytes in vivo.
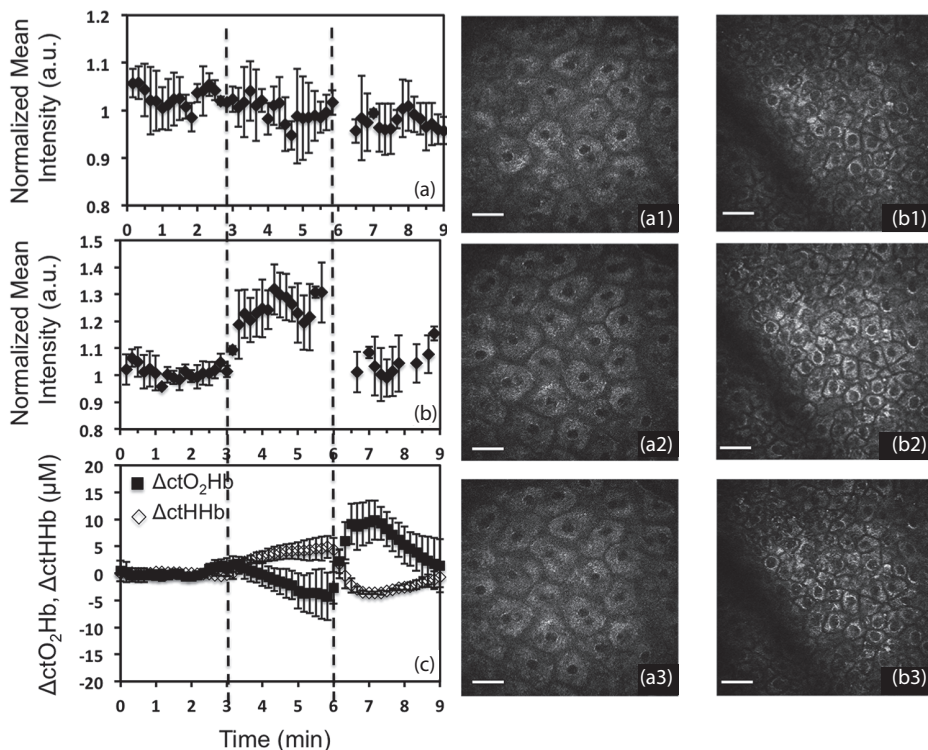

Fig. 15.3: Normalized mean intensity of TPEF images as a function of time before, during and after arterial occlusion for human keratinocytes in stratum granulosum (a) and in a layer close to stratum basale (b). Representative TPEF in vivo images recorded before (a1, b1), during (a2, b2) and after (a3, b3) occlusion corresponding to human keratinocytes in stratum granulosum (a1, a2, a3) and in a layer close to stratum basale (b1, b2, b3). Scale bar is 20 μm. (c) Hemodynamic response to arterial occlusion; oxyhemoglobin concentration ctO$_2$Hb (square), deoxyhemoglobin concentration ctHHb (diamond). The dashed lines represent the start and the release points of the occlusion. Error bars represent standard deviation of five measurements. Reproduced with permission from [7].
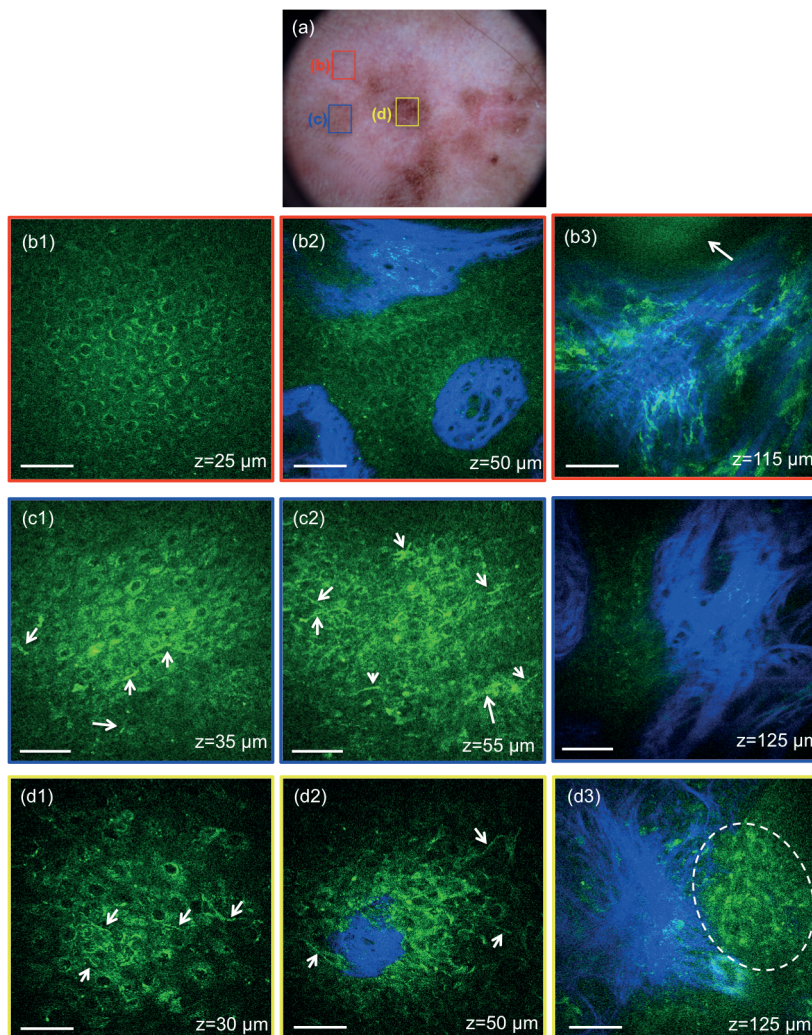
Fig. 15.4: MPM images of a micro-invasive melanoma lesion on a patient's forehead (a) Clinical image (DermLite FOTO, Dermlite Inc.). The markers represent the locations where the images shown in (b1–b3), (c1–c3) and (d1–d3) were acquired. (b1–b3) MPM images corresponding to normal skin adjacent to lesion (red square in (a)) showing normal distribution of keratinocytes (b1), the basal cells (green) surrounding dermal papilla (blue) at 50 μm depth (b2) and collagen (blue) and elastin (green) fibers surrounding a hair follicle (arrow) in the dermis at a depth of 115 μm (b3). (c1–c2) MPM images of the epidermal layers corresponding to different depths of the lesion area indicated by the blue square in (a). The images show ascending melanocytes (white arrows) (c1–c2) and no obvious features of malignancy in the papillary dermis (c3). (d1–d3) MPM images of the lesion area indicated by the yellow square in (a). The images show ascending melanocytes (white arrows) in upper epidermal layers (d1), proliferation of melanocytes (white arrows) at DEJ (d2) and of pigmented cells with different shapes and enlarged nuclei (cellular atypia) in the dermis at a depth of 125 μm. Scale bar is 40 μm. Reproduced with permission from [17].

15.3.3 In vivo MPM imaging of melanoma

Melanoma is the most severe form of skin cancer. It arises from melanocytes, the cells responsible for producing pigment. There are several subtypes of melanoma. Their features have differences and similarities, but generally the following are suggestive of malignancy: presence of melanocytes within the upper portion of the epidermis singly or in groups (Pagetoid spread); irregular junctional activity (atypical melanocytes, architectural disorder); and invasion of tumor cells into the dermis [9, 26, 27]. These features have been identified in melanoma lesions in a study published in 2009, where a DermaInspect MPM tomograph was used to establish sensitivity and specificity criteria for melanoma diagnosis [8]. The assessment by different observers of these features led to overall sensitivity and specificity values for melanoma diagnosis of 75 % and 80 %, respectively. In that study as well as in most of the RCM studies on in vivo imaging of melanoma, particular features of atypical/dysplastic nevi are not extensively discussed.

In a more recent pilot study, our group employed MPM (MPTflex, JenLab, Germany) to identify characteristic features of 15 melanocytic nevi at three different stages: common nevi without dysplastic changes, dysplastic nevi with structural and architectural atypia, and melanoma (5 in each group) [9]. We proposed and developed a quantitative approach by translating the qualitative features used by dermatopathologists in histopathology into quantitative parameters that can be uniquely extracted from 3D in vivo MPM images. We defined a numerical "multiphoton melanoma index (MMI)" based on 3D in vivo image analysis that scores signals derived from TPEF, SHG, and melanocyte morphology features on a continuous 9-point scale. Indices corresponding to common nevi (0–1), dysplastic nevi (1–4) and melanoma (5–8) were significantly different ($p < 0.05$), suggesting the potential of the method to distinguish between melanocytic nevi in vivo [9]. Although promising, a more comprehensive study of a larger number of patients is necessary in order to validate the proposed scoring algorithm and evaluate how well MPM technology can distinguish dysplastic nevi from common nevi and melanoma.

Fig. 15.4 illustrates representative MPM images of a micro-invasive melanoma lesion along with the MPM images corresponding to normal skin adjacent to lesion. The lesion was imaged prior to biopsy. The intraepidermal proliferation of melanocytes and the upward intraepithelial spread shown in the MPM images of Fig. 15.4 were confirmed by histopathology.

15.3.4 In vivo MPM imaging of basal cell carcinoma (BCC)

BCC is a form of skin cancer that originates from the basal cells of the epidermis and associated follicular structures. Nonmelanoma skin lesions, such as BCC have been imaged in vivo by MPM only recently in two pilot research clinical studies [10, 28].

In a first pilot study evaluating the in vivo MPM imaging of BCC lesions, the identi-fied features were compared to the ones provided by RCM imaging [28]. Besides the two main features: elongated, polarized nuclei and tumor nests showing peripheral palisading identified by both techniques, MPM had the ability to evaluate changes in the nucleus/cytoplasm ratio and in cell density across the epidermal layers of BCC le-sions. In a more recent study, the MPM (MPTflex, JenLab, Germany) was used in order to evaluate whether histopathologic criteria can be identified in MPM images [10]. In this study, the MPTflex articulating arm allowed imaging of lesions on different parts of the body rather than being limited to lesions on the extremities, as in the previous work with the DermaInspect [28]. This demonstrated the ability of MPM to identify the main histopathologic criterion for BCC diagnosis in all the lesions imaged: tumor nests of basaloid cells at the DEJ and/or in the dermis that often showed palisading. The ability of MPM to resolve cellular structures inside tumor nests is critical for distin-guishing BCC from other types of neoplasms that involve the presence of nests in the dermis. Fig. 15.5 shows representative MPM images of a BCC lesion imaged by MPM.
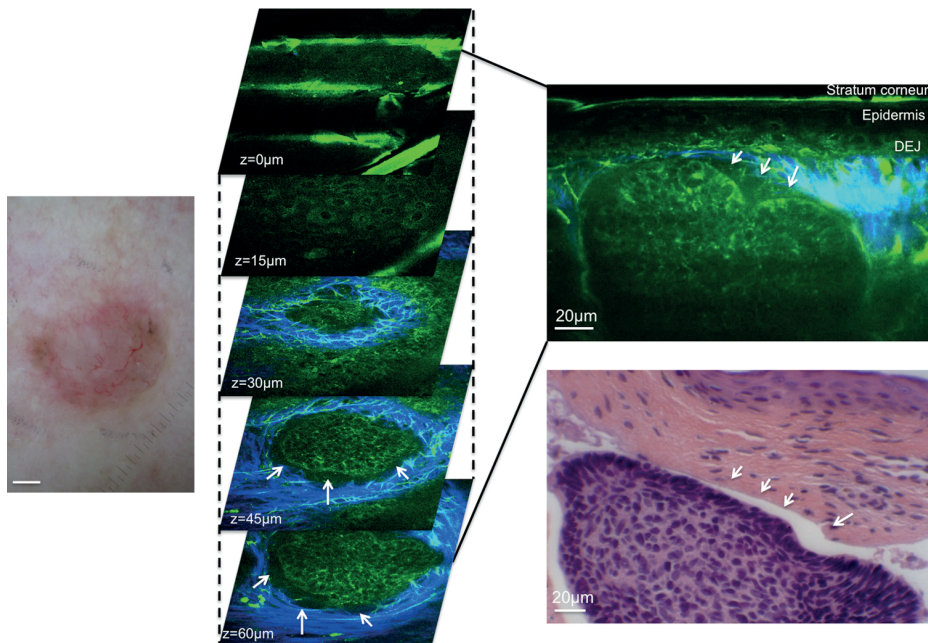

Fig. 15.5: MPM images of a superficial BCC lesion on the shoulder of a patient. (a) Clinical image (DermLite FOTO, Dermlite Inc.), scale bar is 2 mm. (b1–b5) MPM en-face images (XY scans) of the stratum corneum at $z = 0\,\mu m$ (b1), keratinocytes in the stratum spinosum at $z = 15\,\mu m$ (b2), a nest of basaloid cells (green) surrounded by collagen (blue) and elastin fibers (green) imaged at different depths: $z = 30\,\mu m$, 45 μm, 60 μm (b3–b5). (c) Cross-sectional view (XZ scan) corresponding to a vertical plane through the same interrogating volume shown on the left. (d) H & E stained histologic section of the lesion. Both the MPM and the histologic images show a mucinous stroma adjacent to the tumor mass (arrows). Reproduced with permission from [10].

15.3.5 Other applications of MPM in dermatology

Aside from melanoma and nonmelanoma skin cancers, MPM clinical tomographs have also been employed to image other skin conditions such as actinic keratosis [29, 30], atopic dermatitis [31] and pemphigus vulgaris [29]. The morphological features identified in actinic keratosis lesions were associated with wide intercellular spaces between keratinocytes, an increase in the ratio of nuclear to cellular size of keratinocytes and an increase in epidermal thickness compared to adjacent normal skin [30]. In atopic dermatitis lesions, changes in the cellular metabolism of the lesions have been assessed in vivo through protein-bound and free NADH fluorescence lifetime measurements [31].

Monitoring the effects of skin treatments, a key area of focus in the cosmetic industry, is another field of interest for MPM imaging. In a study published in 2010, Bazin et al. used a DermaInspect MPM tomograph to evaluate the effects of a cosmetic product (topical cream) on the collagen and elastin fibers of the forearms of 24 subjects [12]. The ratios between the signals from collagen and elastin were measured at different depths in the dermis for each subject. After 12 weeks of treatment, an increase in the collagen/elastin ratio was measured for the cosmetic product containing active components (soy and jasmine) known to increase collagen synthesis. The treatment with a placebo topical cream (no active ingredients) resulted in no significant variation in the collagen/elastin ratio over the same treatment period of time.

In order to evaluate cosmetic treatments targeting skin anti-aging, approaches to quantify skin aging non-invasively have been investigated by using MPM imaging. Lin et al. proposed a dermis index that estimates the skin age by the ratio of the SHG signal from collagen and the TPEF signal from elastin [32]. The correlation of this index with age was demonstrated by in vivo MPM measurements of sites on subjects' forearms and faces using a DermaInspect tomograph [13, 15]. Kaatz performed depth-resolved measurements of the proposed dermis index and its correlation with age [14]. MPM imaging has also been used by Koehler et al. to evaluate in vivo and non-invasively dermal elastosis, a characteristic of skin photoaging [16].

15.4 Discussion

The development of clinical MPM technologies has led to new, label-free approaches for non-invasive, in vivo imaging of human skin. Recent studies have shown that MPM can be used to assess a wide range of biological processes, including cancer, cellular metabolism, and the effects of skin treatments. While these are promising results indicating that real-time non-invasive "optical biopsies" can be performed at the bedside, translation of this technology into clinical practice is limited by several technical and practical challenges.

In this early stage of MPM technology clinical translation, the limited field of view (about $250 \times 250\,\mu m^2$) and penetration depth (about $200-300\,\mu m$) are the main technical hurdles. The field of view can be increased by implementing a mosaic "tiling" feature (acquisition of adjacent fields of view) or by re-design of optical components such as the tube lens, the scan lens, and the objective. This technical limitation is being addressed by combining tiling with improved lens design in an MPM platform we have recently developed [33]. Penetration depth can be improved by employing dispersion compensation to decrease the laser pulse duration, but the gain would be limited. Generally, this technology is intended as an aid for dermatologists to improve their clinical diagnosis of early stage skin diseases when the uncertainty of their decision is likely to be higher than in the case of advanced disease.

Practical challenges are also related to the need to establish a correlation between MPM and histological images. This is due to the fact that MPM provides high-resolution images of horizontal ($x-y$) optical sections within a tissue. In histopathology, histological cross-sections ($x-z$) of the biopsied tissue are used for diagnosis. In addition, while MPM provides images of cells and extracellular matrix in 3D intact tissue, histological sections contain artifacts due to tissue sectioning, processing, and staining. A relevant example is the different appearance of melanocytes in vivo vs sections. In non-invasive MPM images they have easily detectable dendritic processes that can extend from the cell body into the upper epidermis while in hematoxylin and eosin (H & E) stained histological sections they appear in well-defined lacunae as highly pigmented cells due to a fixation retraction artifact [34]. Finally, the different colors of MPM and histology images might also be a barrier to clinical acceptance of MPM. In MPM, images are usually color-coded using red, green and blue to represent TPEF (red and green) and SHG (blue) signals. Histology is based on stains and images that have real color. For instance, H & E histology is based on two stains (hematoxylin for nuclei, eosin for cellular cytoplasm and extracellular matrix of dermis) and the images appear purple and pink. This potential barrier can be addressed by "digitally staining" the MPM images to mimic the appearance of histology [35]. Generally, overcoming these practical challenges related to translation of MPM in clinical practice requires training by both microscopy specialists and dermatopathologists in order to generate a common language that eases communication.

References

[1]   König K, Riemann I. High-resolution multiphoton tomography of human skin with sub-cellular spatial resolution and picosecond time resolution. Journal of Biomedical Optics. 2003;8(3):432–439.

[2]   Denk W, Strickler JH, Webb WW. Two-photon laser scanning fluorescence microscopy. Science. 1990;248(4951):73–76.

[3]   Campagnola PJ, et al. High resolution non-linear optical microscopy of living cells by second harmonic generation. Biophys J. 1999;77:3341–3349.

[4]   Masters BR, So PT, Gratton E. Multiphoton excitation fluorescence microscopy and spectroscopy of in vivo human skin. Biophys J. 1997;72(6):2405–2412.

[5]   Masters BR, So PT, Gratton E. Multiphoton excitation microscopy of in vivo human skin. Functional and morphological optical biopsy based on three-dimensional imaging, lifetime measurements and fluorescence spectroscopy. Ann N Y Acad Sci. 1998;838:58–67.

[6]   Masters BR, So PT, Gratton E. Optical biopsy of in vivo human skin: Multi-photon excitation microscopy. Lasers in Medical Science. 1998;13(3):196–203.

[7]   Balu M, et al. In vivo multiphoton NADH fluorescence reveals depth-dependent keratinocyte metabolism in human skin. Biophysical J. 2013;104(1):258–267.

[8]   Dimitrow E, et al. Sensitivity and specificity of multiphoton laser tomography for in vivo and ex vivo diagnosis of malignant melanoma. Journal of Investigative Dermatology. 2009;129(7):1752–1758.

[9]   Balu M, et al. Distinguishing between benign and malignant melanocytic nevi by in vivo multiphoton microscopy. Cancer Res. 2014;74(10):2688–2697.

[10] Balu M, et al. In vivo multiphoton microscopy of basal cell carcinoma. JAMA Dermatol. 2015;151(10):1068–1074.

[11] Dancik Y, et al. Use of multiphoton tomography and fluorescence lifetime imaging to investigate skin pigmentation in vivo. Journal of Biomedical Optics. 2013;18(2).

[12] Bazin R, et al. Clinical study on the effects of a cosmetic product on dermal extracellular matrix components using a high-resolution multiphoton tomograph. Skin Res Technol. 2010;16(3):305–310.

[13] Koehler MJ, et al. In vivo assessment of human skin aging by multiphoton laser scanning tomography. Opt Lett. 2006;31(19):2879–2881.

[14] Kaatz M, et al. Depth-resolved measurement of the dermal matrix composition by multiphoton laser tomography. Skin Res Technol. 2010;16(2):131–136.

[15] Sugata K, et al. Evaluation of photoaging in facial skin by multiphoton laser scanning microscopy. Skin Res Technol. 2011;17(1):1–3.

[16] Koehler MJ, et al. Non-invasive evaluation of dermal elastosis by in vivo multiphoton tomography with autofluorescence lifetime measurements. Exp Dermatol. 2012;21(1):48–51.

[17] Balu M, Tromberg BJ. Multiphoton microscopy for non-invasive optical biopsy of human skin. Romanian Journal of Clinical and Experimental Dermatology. 2015;2(3):160–166.

[18] Chance B, et al. Basic principles of tissue oxygen determination from mitochondrial signals. Advances in Experimental Medicine and Biology. 1973;37A:277–292.

[19] Lehninger AL, Nelson DL, Cox MM. Lehninger principles of biochemistry. 5th edition. New York: W.H. Freeman; 2008.

[20] Stucker M, et al. The cutaneous uptake of atmospheric oxygen contributes significantly to the oxygen supply of human dermis and epidermis. Journal of Physiology. 2002;538(3):985–994.

[21] Ronquist G, et al. Human epidermal energy metabolism is functionally anaerobic. Experimental Dermatology. 2003;12(5):572–579.

[22] Cuccia DJ. Spatial frequency domain imaging (SFDI): a technology overview and validation of an LED-based clinic friendly device. Proc SPIE 8254; 2012. p. 825405–825406.

[23] Mazhar A, et al. Wavelength optimization for rapid chromophore mapping using spatial frequency domain imaging. Journal of Biomedical Optics. 2010;15(6):061716.

[24] Nishidate I, et al. Noninvasive imaging of human skin hemodynamics using a digital red-green-blue camera. Journal of Biomedical Optics. 2011;16(8):086012.

[25] Boas DA, Franceschini MA. Haemoglobin oxygen saturation as a biomarker: The problem and a solution. Phil Trans Royal Soc. A Math Phys Eng Sci. 2011;369(1955):4407–4424.

[26] Lever WF, Schaumburg-Lever G. Histopathology of the skin. Sixth edition: Melanocytic nevi and malignant melanoma. Lippincott Williams and Wilkins; 1990.

[27] McKee PH, Calonje E, Granter SR. Pathology of the skin, vol. 2: Melanocytic nevi. 3rd edition. Philadelphia: Mosby; 2005. p. 1250–1258.

[28] Ulrich M, et al. In vivo detection of basal cell carcinoma: comparison of a reflectance confocal microscope and a multiphoton tomograph. J Biomed Opt. 2013;18(6):61229.

[29] Koehler MJ, et al. Clinical application of multiphoton tomography in combination with confocal laser scanning microscopy for in vivo evaluation of skin diseases. Exp Dermatol. 2011;20(7):589–594.

[30] Koehler MJ, et al. Keratinocyte morphology of human skin evaluated by in vivo multiphoton laser tomography. Skin Res Technol. 2011;17(4):479–486.

[31] Huck V, et al. Intravital multiphoton tomography as an appropriate tool for non-invasive in vivo analysis of human skin affected with Atopic Dermatitis. Photonic Therapeutics and Diagnostics Vii. 2011;7883.

[32] Lin SJ, et al. Evaluating cutaneous photoaging by use of multiphoton fluorescence and second-harmonic generation microscopy. Optics Letters. 2005;30(17):2275–2277.

[33] Balu M, et al. Large field of view multiphoton microscopy of human skin. Proceedings SPIE; 2016. Multiphoton microscopy in the biomedical sciences XVI.

[34] McKee PH, Calonje E, Granter SR. Pathology of the skin, Vol. 2: Melanocytic nevi. 3rd edition. Philadelphia: Mosby; 2005. p. 1288.

[35] Bini J, et al. Confocal mosaicing microscopy of human skin ex vivo: spectral analysis for digital staining to simulate histology-like appearance. Journal of Biomedical Optics. 2011;16(7):076008.